Powder Technology 340 (2018) 208–216

Contents lists available at ScienceDirect

Powder Technology

journal homepage: www.elsevier.com/locate/powtec

Process intensification for scalable synthesis of ytterbium and erbium co-doped sodium yttrium fluoride upconversion nanodispersions

Yuan Pu [a,b], Jingning Leng [a,b,c], Dan Wang [a,b,*], Jie-Xin Wang [a,b], Neil R. Foster [b,d], Jian-Feng Chen [a,b]

[a] Research Center of the Ministry of Education for High Gravity Engineering and Technology, Beijing University of Chemical Technology, Beijing 100029, China
[b] State Key Laboratory of Organic-Inorganic Composites, Beijing University of Chemical Technology, Beijing 100029, China
[c] Solartron Technology Co., Ltd., Ningbo, Zhejiang 315031, China
[d] Department of Chemical Engineering, Curtin University, Perth, WA 6845, Australia

ARTICLE INFO

Article history:
Received 25 July 2018
Received in revised form 5 September 2018
Accepted 15 September 2018
Available online 17 September 2018

Keywords:
Intensified mixing
Upconversion luminescence
Transparent nanodispersion
Rotating packed bed
Anti-counterfeiting

ABSTRACT

Rare-earth doped $NaYF_4$ upconversion nanomaterials have found many applications from biosensing through photoelectric conversion to luminescent anti-counterfeiting. However, the scalable synthesis methods of ultrasmall $NaYF_4$ nanoparticles are still challenging. Herein, We demonstrated that the intensified mixing of the precursor by a high-gravity rotating packed bed (RPB) reactor before the hydrothermal synthesis process enabled the preparation of ultrasmall $NaYF_4$:Yb^{3+}/Er^{3+} upconversion nanoparticles, with much smaller size, more uniform distributions and higher Er^{3+}-doping level than those obtained in the stirred tank reactor (STR) route. In stark contrast to conventional synthetic techniques that require stringent control over several experimental variables for controlling morphologies and sizes, the process intensification approach presented here requires modification of only a single variable while enabling tremendous improvements to control the formation of $NaYF_4$ based UCNPs with small feature size. The UCNPs dispersed well in various organic solvents (e.g. ethanol, acetone, toluene, cyclohexane, etc.), forming transparent nanodispersions with upconversion luminescence under 980 nm NIR light irradiation. The preliminary applications of $NaYF_4$:Yb^{3+}/Er^{3+} nanodispersions for upconversion luminescent transparent hybrid films and anti-counterfeiting were also demonstrated.

1. Introduction

Rare-earth doped upconversion nanoparticles (UCNPs) that convert longer wavelength NIR light into shorter wavelength ultraviolet/visible/NIR light have attracted extensive scientific attention in recent years [1–4]. After several decades of technological developments, UCNPs have found many applications in many fields such as anti-counterfeiting [5–7], optoelectronic devices [8], bioimaging [9,10] and cancer treatment [11,12]. For instance, both theoretically and experimental studies have demonstrated that the power conversion efficiency of a solar cell would be significantly increased by using an ideal upconverter, such as transparent hybrid films embedded with UCPNs [13–15]. In addition, UCNPs have recently shown great potential to satisfy the demands for anti-counterfeiting applications due to their small size, low power density NIR excitation, high chemical stability, good wetting properties and compatibility with transparent security inks [5–7,16]. Since the traditional anti-counterfeit technologies are easily infringed [17], an advanced anti-counterfeit technology is therefore urgently needed in many important fields, especially for anti-counterfeit of paper documents or certificates, such as checks, passports, and even banknotes [16,18]. The efforts of chemical engineers are to develop solutions for some important problems, including but not limited to design, operation, control, optimization, and intensification of chemical, physical, and biological processes for sustainable development [19]. Upconversion luminescence based anti-counterfeiting is one of the most promising directions in moving toward UCNPs for large-scale production and commercial applications. It has been generally accepted that ultrasmall UCNPs are beneficial for hybrid optoelectronic devices and anti-counterfeiting ink. Therefore, the development of scalable methods for the synthesis sub-10 nm UCNPs is one of key materials challenge.

UCNPs are typically composed of an inorganic host lattice and rare-earth dopant ions embedded in the host lattice [4]. Sodium yttrium fluoride ($NaYF_4$) is among the most effective host materials for upconverison luminescence process due to its lowest phonon energy (phonon cutoff ~350 cm^{-1}), low nonradiative decay rates, and high radiative emission rates, especially doping with Yb^{3+}/Er^{3+} and Yb^{3+}/Tm^{3+} [3]. One common synthetic method for $NaYF_4$:Yb^{3+}/Er^{3+} nanoparticles is based on the thermal decomposition of trifluoroacetate precursors in high boiling noncoordinating solvents [20,21]. However, the thermal decomposition approach requires expensive precursors and

* Corresponding author at: Research Center of the Ministry of Education for High Gravity Engineering and Technology, Beijing University of Chemical Technology, Beijing 100029, China.
E-mail address: wangdan@mail.buct.edu.cn (D. Wang).

https://doi.org/10.1016/j.powtec.2018.09.035
0032-5910/

high energy consumption, which limited the scale-up production of UCNPs. Another approach for preparation of $NaYF_4$:Yb^{3+}/Er^{3+} nanoparticles is based on liquid precipitation reaction between soluble rare-earth salts and alkali fluorides along with post hydrothermal process [22,23], which has been regarded as an effective method for mass production of UCNPs due to the low-cost and ease of scale-up. However, it is a common problem that the rare-earth doped $NaYF_4$ sample prepared shows two distinct particle morphologies that include small nanocubes and large nanorods, making it hard to obtain products with uniform size and well-proportioned distribution. The conventional precipitation process is usually performed in a batch-type stirred tank reactor (STR), in which the nucleation of UCNPs does not take place uniformly due to the low efficiency of mass transfer and fluid mixing in STR [24,25]. In 2010, Wang et al. reported a route for synthesis of ultra-small $NaYF_4$ based UCNPs with uniform morphology by doping Gd^{3+} ions, making a breakthrough in this field [26]. Simultaneous phase and size control of $NaYF_4$ based UCNPs through lanthanide doping lead to another issue, namely the additional of extra reactants and ions in the nanocrystal, raising the costs of raw materials and reducing the performance of the products.

Herein, we propose a route for the synthesis of $NaYF_4$:Yb^{3+}/Er^{3+} UCNPs by utilizing a high gravity rotating packed bed (RPB) reactor for nucleation of UCNPs along with post hydrothermal process. The high gravity environment and tiny droplets generated by the RPB lead to significant intensification of mass transfer and micromixing, which are of great benefit for the homogeneous nucleation and growth of particles [27,28]. Detailed studies on the effects of operating parameters and comparison with those obtained via a traditional STR route. The morphology, structure and upconversion luminescence property of the $NaYF_4$: Yb^{3+}/Er^{3+} nanoparticles were investigated by transmission electron microscope (TEM), power X-ray diffraction (XRD), Fourier transform infrared (FTIR) spectrophotometry and luminescence spectra measurements. The upconversion luminescence behaviors of $NaYF_4$:Yb^{3+}/Er^{3+} nanoparticles dispersed in various organic solvents were investigated. Furthermore, transparent hybrid films of $NaYF_4$:Yb^{3+}/Er^{3+} and polyvinyl butyral (PVB), which has been among the most widely used binders for inks, were prepared by solution blending method. The $NaYF_4$:Yb^{3+}/Er^{3+} nanoparticles were also transferred into aqueous phase and used as the ink to draw anti-counterfeiting watermarks in paper. Upconversion luminescence properties of the hybrid films and the papers under the irradiation of 980 nm NIR laser were also investigated, demonstrating the potential of the $NaYF_4$:Yb^{3+}/Er^{3+} nanodispersions for anti-counterfeiting.

2. Experimental section

2.1. Materials

Yttrium chloride hexahydrate ($YCl_3{\cdot}6H_2O$, 99.9%), ytterbium chloride hexahydrate ($YbCl_3{\cdot}6H_2O$, 99.9%), erbium chloride hexahydrate ($ErCl_3{\cdot}6H_2O$, 99.5%), were purchased from Macklin Biochemical Co., Ltd. (Shanghai, China). Oleic acid, sodium hydroxide, ammonium fluoride (NH_4F) and organic solvents were purchased from Sinopharm Chemical Reagent Co., Ltd. (Beijing, China). 1,2-distearoylsn-glycero-3-phosphoethanolamine-N-[methoxy(polyethyleneglycol)-5000] (PEG) was purchased from Creative PEGWorks, Inc. The polyvinyl butyral (PVB) resin was obtained from the Sigma Aldrich. All the chemicals were used without any additional purification unless otherwise mentioned. Deionized water prepared by a Hitech Laboratory Water Purification System DW100 (Shanghai Hitech Instruments Co., Ltd.) was used for all experiments.

2.2. Synthesis of $NaYF_4$: Yb^{3+}/Er^{3+} by STR route

For the synthesis of $NaYF_4$:Yb^{3+}/Er^{3+} nanodispersions in a common STR reactor, 6 mL of NaOH aqueous solution (0.01 mol/mL) was mixed with 40 mL of oleic acid under vigorous stirring, forming oil-water mixture solution A. The solution B which is 22 mL of aqueous solution containing 2.56 mmol of $YCl_3{\cdot}6H_2O$, 0.576 mmol of $YbCl_3{\cdot}6H_2O$, and 0.064 mmol of $ErCl_3{\cdot}6H_2O$, was added into the solution A under vigorous stirring, followed by the addition of 16 mL of solution C (i.e. aqueous solution of NH_4F with concentration of 1 mol/L). After stirring at room temperature for 15 min, the mixed solution was sealed into a Teflon-lined autoclave and heated at 200 °C for 2 h. As the solution cooled to room temperature, the paste of $NaYF_4$:Yb^{3+}/Er^{3+} was collected by centrifugation and washing for 4 times with water and ethanol, respectively. The $NaYF_4$:Yb^{3+}/Er^{3+} nanodispersions were then obtained by re-dispersing the paste in organic solvents (e.g. ethanol, acetone, ethyl acetate, toluene, cyclohexane, etc.) under ultrasonic treatment.

2.3. Synthesis of $NaYF_4$: Yb^{3+}/Er^{3+} by RPB route

In order to investigate the effect of process intensification of high-gravity technology on the preparation of $NaYF_4$:Yb^{3+}/Er^{3+} nanodispersions, a RPB reactor was used to mix the three kinds of formulated solution (solution A, B, and C) instead of mixing them in a STR. The RPB reactor consists of a rotator with stainless packing, two liquid inlets, an outlet, a casing, and a motor, and the detailed setup information on the RPB reactor can be found in our previous work [29]. The dosage and the volume of reactants were the same as those of the STR experiment. The solution A, containing 0.06 mol of NaOH, 6 mL of water, 40 mL of ethanol, and 40 mL of oleic acid, were pumped into RPB reactor through one feed inlet. The solution B (22 mL of aqueous solution containing 2.56 mmol of $YCl_3{\cdot}6H_2O$, 0.576 mmol of $YbCl_3{\cdot}6H_2O$, and 0.064 mmol of $ErCl_3{\cdot}6H_2O$) and solution C (16 mL of 1 mol/L NH_4F aqueous solution) were pumped into the RPB reactor through the other feed inlet. The post hydrothermal process of the RPB route was the same as the STR experiment. In our experiment, we explored the influence of the different high-gravity level on the particle size of the UCNPs nanoparticles by changing the rotation speeds of the RPB from 1000 to 2500 rpm. As calculated by Eq. 1 [28], the high gravity levels (β) of the RPB routed at various rotation speeds (1000, 1500, 2000, and 2500 rpm) were determined to be 70 g, 157 g, 279 g, and 436 g, respectively.

$$\beta = \frac{\omega^2 r}{g} \tag{1}$$

where β is the high gravity level. The ω is he angular speed of the RPB reactor. The r is the geometric average radius of the rotator and g represents the gravitational acceleration speed (i.e. 9.8 m/s^2).

2.4. Phase-transfer of $NaYF_4$: Yb^{3+}/Er^{3+} nanoparticles

The phase-transfer $NaYF_4$:Yb^{3+}/Er^{3+} nanoparticles into aqueous solution was performed by a simple phase inversion method as reported in the previous work with some modifications [30]. Briefly, 2 mL of $NaYF_4$:Yb^{3+}/Er^{3+} nanodispersions in chloroform (10 mg/mL) and 2 mL of PEG solution in chloroform (10 mg/mL) were mixed. The mixture solution was gently heated at 50 °C in a rotary evaporator to evaporate the chloroform. Next, 5 mL of water was added to the solid mass followed by ultrasonic treatment for 5 min. The excess PEG molecules were removed by centrifugal separation and the final product of PEG coated $NaYF_4$:Yb^{3+}/Er^{3+} nanoparticles were re-dispersed in 10 mL of water for further use.

2.5. Characterization

XRD patterns of the samples were measured by a Shimadzu XRD-6000 diffractometer. The FTIR spectra of solid samples were measured by a PerkinElmer spectrum GX Fourier system. The morphology studies of the nanoparticles were performed using a Hitachi H-9500 TEM. The

particle size distribution of the samples obtained from TEM images were measured using ImageJ. The thermogravimetric analysis (TGA) was performed using a Q50 therm-gravimetric analyzer in the temperature range of 30–600 °C in air atmosphere. Upconversion luminescence spectra of the samples were acquired on a PG2000 spectrometer (Ideaoptics Instruments, China) equipped with a commercial 980 nm laser. The transmissivities of $NaYF_4$:Yb^{3+}/Er^{3+}-PVB films were characterized by a Shimadzu UV-2600 UV-vis spectrometry.

3. Results and discussion

3.1. Formation of $NaYF_4$: Yb^{3+}/Er^{3+} nanoparticles

Although the synthesis of $NaYF_4$:Yb^{3+}/Er^{3+} UCNPs by hydrothermal route has been intensively investigated, the chemical reaction and process have rarely been put forward in previous literatures [1,26]. In Fig. 1a, the major process involved in the formation of $NaYF_4$:Yb^{3+}/Er^{3+} nanocrystrals in our route were proposed. Generally, the neutralization reaction of sodium hydroxide and oleic acid was adopted to produce free oleate ions in the oil and water mixture. The rare-earth ions (RE^{3+}) then reacted with the oleate ions via complexation reaction. After the addition of fluorine ions (F^-) in the mixture, the RE^{3+} ions released from the complex and reacted with Na^+ and F^- to form $NaYF_4$ crystal nuclei and then grown up during the hydrothermal treatment. The following reactions occurred during the synthesis process of $NaREF_4$ nanoparticles.

$$C_{17}H_{33}COOH(l) + OH^-(aq) \rightarrow C_{17}H_{33}COO^-(aq) + H_2O(l)$$

$$3C_{17}H_{33}COO^-(aq) + RE^{3+}(aq) \rightarrow (C_{17}H_{33}COO)_3RE(l)$$

$$Na^+(aq) + (C_{17}H_{33}COO)_3RE(l) + F^-(aq) \xrightarrow{\Delta} NaREF_4(s) + 3C_{17}H_{33}COO^-(aq)$$

Due to the coordination of oleic acid with salts of rare-earth metal, the oleic acid adsorbed on the surface of the $NaREF_4$ nanocrystals and suppressed the growth of the primary particles. Since various crystal planes of $NaREF_4$ have different adsorption capacities of oleic acid, leading to the differences of growth speed, the uniform adsorption of oleic acid on the surface of $NaREF_4$ nuclei are critical for the preparation of ultrasmall nanoparticles with uniform size distribution, which requires the homogeneous micromixing of the reactants before the nucleation process. In the common route for the mixing of the precursors using a conversional STR, uniform mixing was hard to realize in all areas of the reactor in a short time (i.e. several milliseconds). Especially in the regions far from the stirring oars, if the homogeneous micromixing was not achieved after the precipitation nucleating of $NaREF_4$, the oleic acid molecules were not enough to cover the surface of the nuclei and the oleic acid selectively binded to some specific panels of the $NaREF_4$ nuclei. Therefore, large nanorods then formed due to the faster growth speed of the panels without oleic acid than those panels adsorbed oleic acid. Fig. 1b shows a typical TEM image of $NaYF_4$:Yb^{3+}/Er^{3+} particles obtained by mixing in the conversional STR coupling with hydrothermal treatment, in which particles with two distinct morphologies including large nanorods and small nanocubes were observed and these results were consistent with the previous literature [26]. Although high-quality UCNPs have been obtained in laboratory scale by precise control of the reaction parameters such as precursor injection speed and stirring rate, it is difficult to control the uniform mixing and mass transfer upon the injection of precursor solutions in STR, which leads to low batch-to-batch reproducibility. This problem will become more prominent in the large-scale production of UCNPs (e.g., tens to hundreds of kilograms).

3.2. High-gravity-assisted synthesis of $NaYF_4$: Yb^{3+}/Er^{3+} nanoparticles

An alternative to a batch reactor, the RPB reactor can generate a high-gravity environment with homogeneous supersaturation, concentration, and temperature, which is of benefit for the homogeneous nucleation and growth of particles. Our previous work demonstrated that the intensified mixing of RPB reactor were beneficial for the preparation of Gd_2O_3 based UCNPs [31]. By using high gravity reactive precipitation along with post calcination methods, the obtained Gd_2O_3 nanoparticles exhibited average size of ~100 nm, which is much smaller than the common route (~350 nm). Compared with the Gd_2O_3 based UCNPs reported in that work [31], the $NaYF_4$ based UCNPs are more

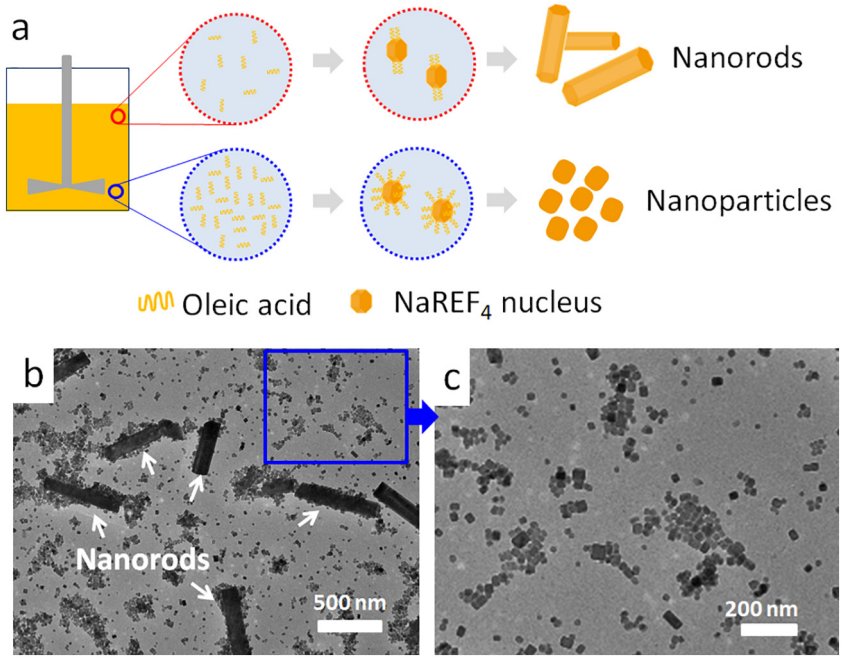

Fig. 1. (a) Schematic diagram of the process involved in the formation of $NaREF_4$ particles. (b) A typical TEM image of the $NaYF_4$:Yb^{3+}/Er^{3+} sample obtained by mixing the precursors in conversional STR coupling with hydrothermal treatment. (c) A magnified shot showed the nanopraticles in (b).

benefit for various applications due to their higher luminescence efficiency, smaller particle size and larger dispersibility in solvents. Meanwhile, the scalable preparation of uniform $NaYF_4$ based UCNPs are more challenging. For instance, the requirement of homogeneous mixing at molecular level in the multicomponent and heterogeneity system (oleic acid, water, metal salts, etc.) is stronger. Based on the understanding of the process and chemical reactions involved in the formation of $NaYF_4$ based UCNPs as mentioned above, we propose a route for the synthesis of $NaYF_4$:Yb^{3+}/Er^{3+} UCNPs by utilizing a RPB reactor for nucleation coupling with hydrothermal process for growth of the nanoparticles. To investigate the effect of high-gravity process intensification on the preparation of $NaYF_4$: Yb^{3+}/Er^{3+} UCNPs, the RPB reactors operated with high-gravity levels of 157 g, 279 g and 436 g were used for the mixing of the precursors. The low magnification TEM images of the samples prepared by RPB routes with high-gravity levels of 157 g, 279 g and 436 g were shown in Fig. 2a–c, in which only small nanocubes were observed. These results demonstrated that the intensified micromixing of the precursors by the RPB reactor are beneficial for the preparation of ultrasmall $NaYF_4$ based nanoparticles. Due to the high-gravity field in the RPB, the liquids going through the packing were spread or split into ultrafine droplets, threads and/or thin films in the porous packing and the mass transfer and micromixing in the mixture containing oleic acid, water and metal salts, could be greatly intensified. The uniform adsorption of oleic acid molecules on the surface of $NaREF_4$ nuclei was achieved during the precipitation nucleating process. Therefore, the uniform surface coating of surfactants on the nuclei provided more restriction on the growth of the nanoparticles, resulting in the formation of small $NaREF_4$ UCNPs. It should be noted that the quality of the UCNPs exhibited in the TEM images could be further improved by purification and/or screening the samples, for example using the supernatant of the UCNPs dispersions for TEM imaging. However, in our work, we focused on the scalable synthesis of $NaREF_4$ based UCNPs and the effects of the intensified mixing by RPB reactors on the formation of UCNPs. The TEM images were used to reflect and express the general morphologies of the particles. These results have clearly demonstrated that there were no large nanorods obtained by using RPB route for the synthesis of UCNPs, which was promising for scalable synthesis of UCNPs with uniform size and well-proportioned distribution. The high magnification TEM images (Fig. 2d–f) and respective diameter analysis (Fig. 2g–i) indicated that the size distribution of $NaYF_4$:Yb^{3+}/Er^{3+} UCNPs obtained by RPB routes was concentrated in the range of 10–20 nm. With increase of high-gravity level of the RPB, the mixing time of the precursor decreased, leading to shorter time for precipitation nucleating and resulting smaller nucleic. Therefore, the average size of the UCNPs obtained decreased as the increase of the high-gravity level.

3.3. Chemical structures of $NaYF_4$: Yb^{3+}/Er^{3+} nanoparticles

The crystal structures and chemical compositions of the $NaYF_4$:Yb^{3+}/Er^{3+} UCNPs synthesized by STR and RPB routes were then investigated by XRD, FTIR and TGA analyses. Fig. 3a shows the XRD patterns

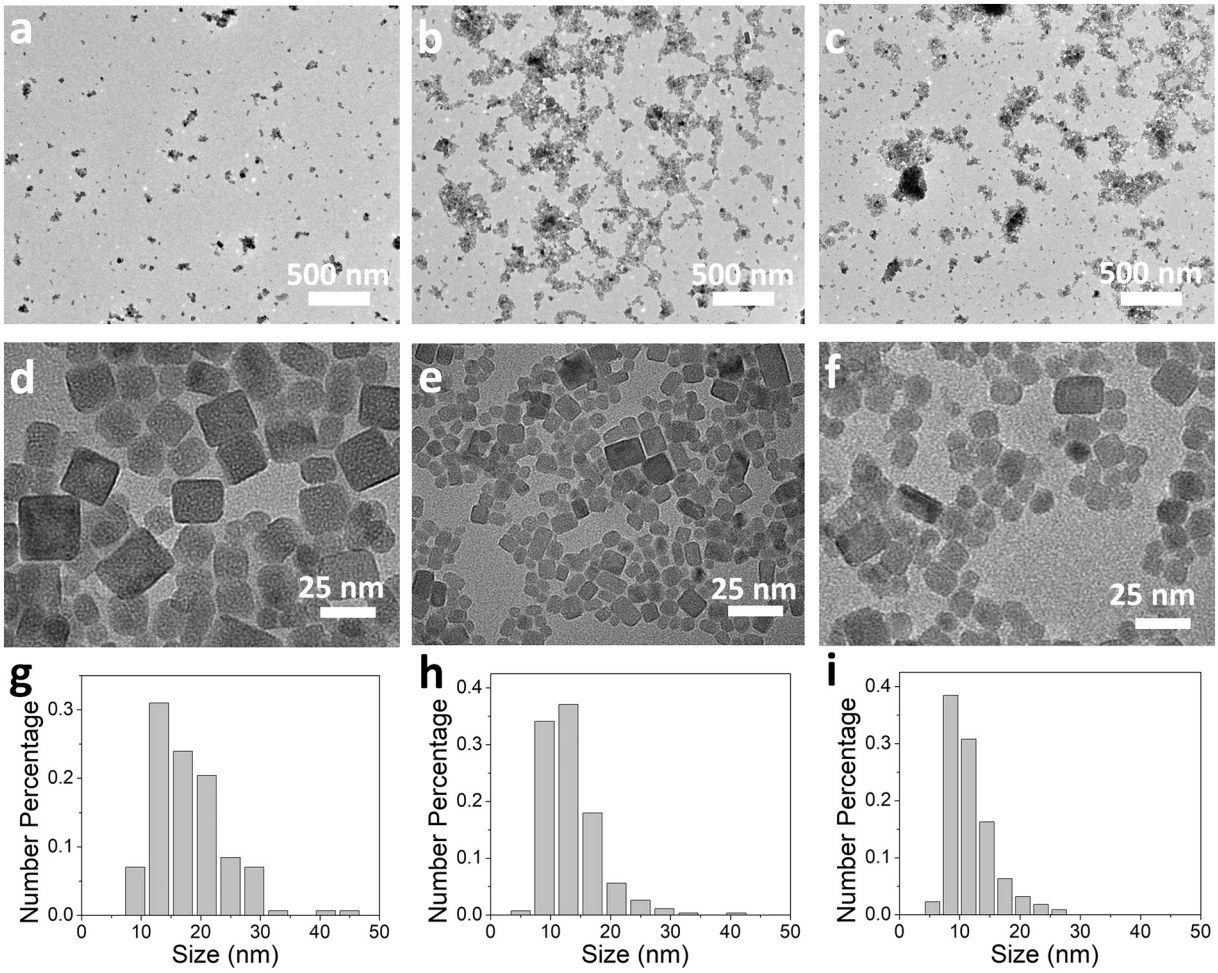

Fig. 2. Low magnification TEM images of the $NaYF_4$:Yb^{3+}/Er^{3+} UCNPs synthesized by RPB route with high-gravity levels of (a) 157 g, (b) 279 g and (c) 436 g. High magnification TEM images of the $NaYF_4$:Yb^{3+}/Er^{3+} UCNPs synthesized by RPB route with high-gravity levels of (d) 157 g, (e) 279 g and (f) 436 g. Size distribution profiles of the $NaYF_4$:Yb^{3+}/Er^{3+} UCNPs synthesized by RPB route with high-gravity levels of (g) 157 g, (h) 279 g and (i) 436 g.

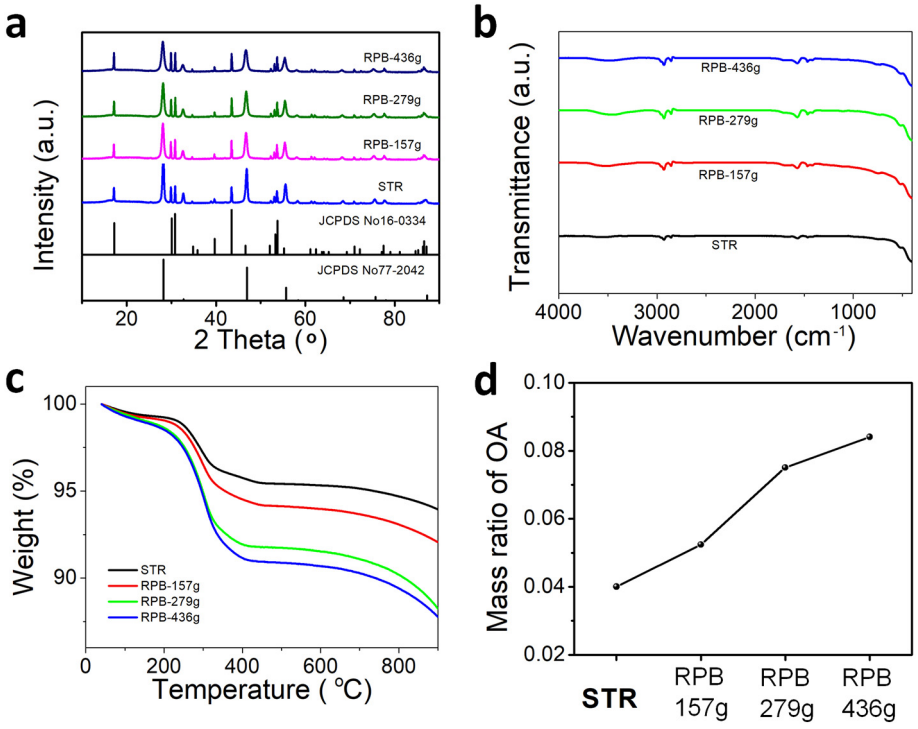

Fig. 3. (a) XRD patterns, (b) FTIR spectra and (c) TGA curves of $NaYF_4$: Yb^{3+}/Er^{3+} samples obtained by the STR route and RPB routes with high gravity level of 157 g, 279 g and 436 g respectively. (d) Weight ratios of the organic oleic acid (OA) molecules in the UCNPs calculated from TGA data.

of the prepared $NaYF_4$:Yb^{3+}/Er^{3+} UCNPs, in which the diffraction peaks of cubic phase (JCPDS 77-2042) and hexagonal phase (JCPDS 16-0334) of $NaYF_4$ were observed from all the four samples, with no impurity peaks. The average crystal sizes of each phase and the mass fractions from each phase in different samples were calculated according to the XRD patterns and the results were shown in Tables 1 and 2, respectively. The average crystal sizes of the samples were a little larger than the average particle size measured by TEM. The difference between the particle sized obtained by XRD and TEM could be attributed to the fact that the XRD results reflect the crystalline particles, not the actual morphology of the particles. Besides, for the measurement of XRD large particles are usually picked, while most of the small particles are counted in TEM images. Nevertheless, the use of RPB and different high-gravity levels showed no significant influence on the average crystal size and the mass fraction from each phase of $NaYF_4$:Yb^{3+}/Er^{3+} UCNPs. It should be noted that $NaYF_4$ contains two phases: cubic and hexagonal phase. The molar ratio of surfactants (oleic acid) and the solvents (ethanol, water) and temperature were key factors for phase control of $NaYF_4$ nanocrystals. The XRD results demonstrated that the micromixing was not ideal homogeneous during the whole process of UCNPs synthesis and there is still room for improvement. Producing phase-pure UCNPs is important since the phase purity defines upconversion properties and should be good topics to follow.

The FTIR spectra in Fig. 3b demonstrated the presence of oleic acid on the surface of the nanoparticles. The absorption peak near 3500 cm^{-1} is the stretching vibration peak of oxhydryl (—OH). The peak at 2927 cm^{-1} and 2853 cm^{-1} were attributed to the asymmetric and symmetric stretching vibration of methylene (CH_2) in the long alkyl chain. The peak at 1563 cm^{-1} was the asymmetric stretching absorption peak of —C═O— in carboxyl (—COOH), and the peak at 1461 cm^{-1} was the characteristic absorption peak of methyl ($—CH_3$). The TGA curves of the samples were shown in Fig. 4c, in which the weight loss below 200 °C were attributed to the loss of water absorbed on the surface of the nanoparticles. The weight reduced between 200–500 °C was caused by the desorption of O—H and the decomposition of oleic acid. The weight ratios of the organic oleic acid molecules to the inorganic $NaYF_4$:Yb^{3+}/Er^{3+} crystals for various samples were calculated according to the TGA data. A general trend was observed that the coating of oleic acid on the surface of $NaYF_4$:Yb^{3+}/Er^{3+} increased as the increasing of the high-gravity levels in the range of 157–436 g (Fig. 4d). The average size of the UCNPs obtained decreased as the increase of the high-gravity level and the surface area of the UCNPs increased, leading to the absorption of more oleic acid molecules.

3.4. Upconversion luminescence properties of $NaYF_4$: Yb^{3+}/Er^{3+} nanoparticles

The upconversion luminescence spectra of the four samples were presented in Fig. 4a and the data were normalized by the luminescence peak at 650 nm. All the luminescence spectra were quite similar in shape with three obvious bands in the range 520–528 nm, 539–550 nm, and 653–661 nm, which correspond to the $^2H_{11/2} \rightarrow {}^4I_{15/2}$, $^4S_{3/2} \rightarrow {}^4I_{15/2}$,and $^4F_{9/2} \rightarrow {}^4I_{15/2}$ transitions of Er^{3+} ions,respectively. Interestingly, the intensity ratio of red to green lights is increased with increasing high gravity levels during the synthesis approaches. The possible upconversion luminescence mechanism of the investigated system was proposed in Fig. 4b. When the sample was excited by 980 nm optical fiber laser, Er^{3+} ions are transferred from the ground

Table 1
Average crystal sizes of each phase in different samples.

Mass fraction (%)	STR	RPB-157 g	RPB-279 g	RPB-436 g
Cubic phase	21.4	14.1	15.6	12.4
Hexagonal phase	62.5	70.4	69.4	77.1

Table 2
Mass fractions of each phase in different samples.

Mass fraction (%)	STR	RPB-157 g	RPB-279 g	RPB-436 g
Cubic phase	85.7	84.7	84.1	85.2
Hexagonal phase	14.3	15.3	15.9	14.8

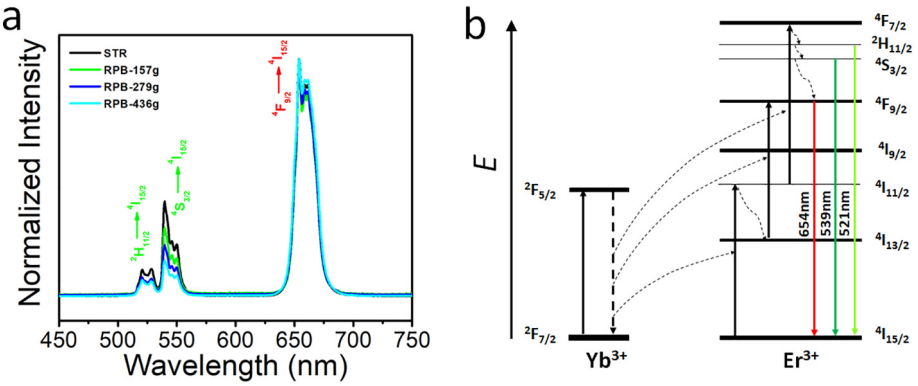

Fig. 4. (a) Normalized upconversion luminescence spectra of various $NaYF_4$:Yb^{3+}/Er^{3+} samples obtained by the STR route and RPB routes with different high gravity level: 157 g, 279 g, and 436 g, respectively. The samples were excited by 980 nm NIR laser (2 W/cm^2) and the spectra data were normalized by the luminescence peak at 650 nm. (b) Upconversion luminescence mechanism of the green and red emission. (For interpretation of the references to colour in this figure legend, the reader is referred to the web version of this article.)

state energy level ($^4I_{15/2}$) to the excited energy level ($^4I_{11/2}$) and Yb^{3+} ions on the ground state ($^2F_{7/2}$) are excited to the excited state ($^2F_{5/2}$), where the energy come from the ground state transfer (GSA) process. The Yb^{3+} will then transfer the energy to the nearby Er^{3+} ions through the energy transfer (ET) process, when the electrons of Yb^{3+} ions return to the ground state ($^2F_{7/2}$). A part of the excited electrons on the $^4I_{11/2}$ level will populate the intermediate level $^4I_{13/2}$ by nonradiative relaxation (NR), and other excited electrons on the $^4I_{11/2}$ level will continue to absorb energy and populate $^4F_{7/2}$ due to the ESA and/or ET. Then, the electrons on the intermediate level $^4I_{13/2}$ will be excited into $^4F_{9/2}$ by ESA and/or second-step ET, and the electrons on the excited state $^4F_{7/2}$ will populate $^2H_{11/2}$, $^4S_{3/2}$, and $^4F_{9/2}$ by NR. At last, the $^2H^{11/2}$ level and $^4S^{3/2}$ level undergo radiative decay to produce green emission 520–528 nm and 539–550 nm, and the $^4F^{9/2}$ level undergoes radiative decay to produce red emission 653–661 nm. For a system with low Er^{3+} concentration, the probability of nonradiative decay from $^4F_{7/2}$ to $^2H_{11/2}$ or $^4S_{3/2}$ is rather large, resulting in the dominant population at $^2H_{11/2}$ or $^4S_{3/2}$ level responsible for the green emission. When the concentration of Er^{3+} in nanocrystals increased, the distances between pairs of Er^{3+} ions in $NaYF_4$ reduce correspondingly, which would lead to the near resonant cross relaxation originating from the interaction of Er^{3+} ions [32], causing the intensity quenching of green emission. Therefore, with the increase of Er^{3+} content in the medium doping range (0.2–2.0%) of Er^{3+}, the green emission tends to trail off, while the red one boosts up accordingly. The spectra in Fig. 4a demonstrated that $NaYF_4$:Yb^{3+}/Er^{3+} particles obtained by RPB routes exhibited higher Er^{3+}-doping levels compared with those prepared by STR route, suggesting that the Er^{3+}-doping levels were enhanced with the increased high-gravity levels.

Fig. 5a shows the digital photos of the $NaYF_4$: Yb^{3+}/Er^{3+} nanodispersions obtained by the RPB route (high gravity level = 279 g) in various organic solvents, including ethanol, acetone, tetrahydrofuran, ethyl acetate, chloroform, toluene, and cyclohexane. The concentrations of the nanoparticles were 1 mg/mL for all the nanodispersions, which were almost transparent. Under the irradiation of 980 nm NIR light, the nanodispersions showed significant visible lines, due to the upconversion luminescence of the $NaYF_4$: Yb^{3+}/Er^{3+} nanoparticles (Fig. 5b). Fig. 5c presents upconversion luminescence spectrum of the nanodispersions, demonstrating that the luminescence properties of the $NaYF_4$:Yb^{3+}/Er^{3+} nanoparticles were stable in various organic solvents of different polarities.

3.5. $NaYF_4$: Yb^{3+}/Er^{3+} nanodispersion for transparent hybrid films

Polyvinyl butyral (PVB) resin has been among the most widely used binders for inks [33]. In this work, we prepared highly transparent PVB/UCNPs nanocomposites via the solvent blending method, by mixing 20 mL of $NaYF_4$: Yb^{3+}/Er^{3+} nanodispersions (0.5 mg/mL in chloroform) with 1 g of PVB followed by the evaporation of the chloroform. Fig. 6a shows typical pictures of a PVB film (1 cm × 1 cm × 100 μm) and a PVB/UCNPs hybrid film (1 cm × 1 cm × 100 μm). Both films were highly transparent as words under the films could be clearly observed. Fig. 6b shows the transmittance spectra of the PVB film and the PVB/UCNPs hybrid films with different mass of UCNPs:PVB (1:100, 3:100, and 5:100).

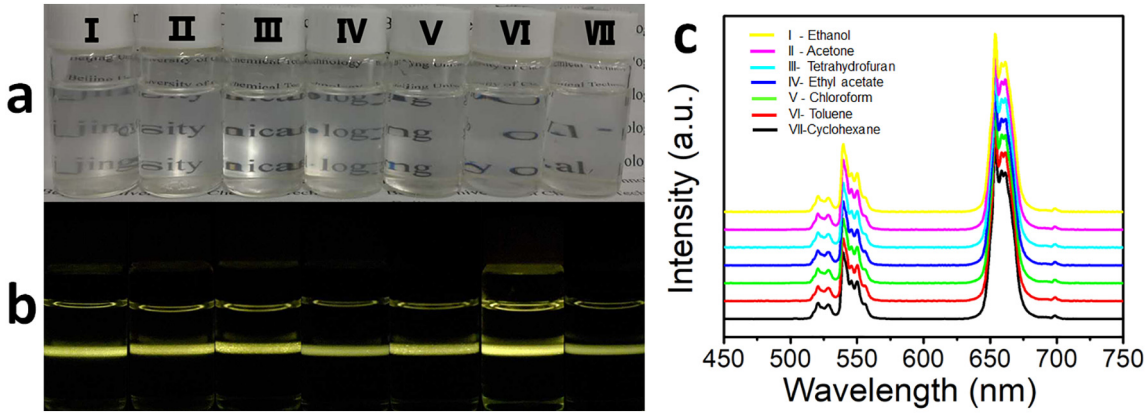

Fig. 5. (a) Photographs of 1 mg/mL $NaYF_4$:Yb^{3+}/Er^{3+} nanodispersions in I: ethanol, II: acetone, III: tetrahydrofuran, IV: ethyl acetate, V: chloroform, VI: toluene and VII: cyclohexane. (b) Luminescence images and (c) spectra of the nanodispersions under the 980 nm laser excitation (normalized by the luminescence peak at 650 nm). The spectra are stacked with a slight offset to interpret clearly.

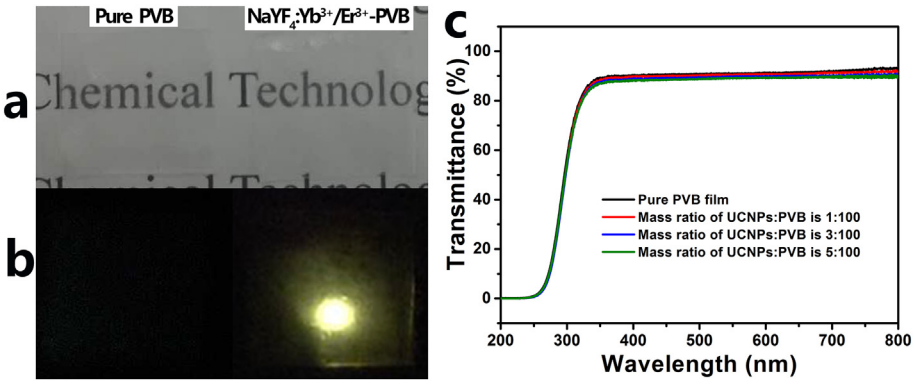

Fig. 6. (a) Digital photographs of a PVB film (1 cm × 1 cm × 100 μm) and a PVB/UCNPs hybrid film (1 cm × 1 cm × 100 μm) under daylight. (b) Transmittance spectra of the PVB film and the PVB/UCNPs hybrid films with different mass ratios of UCNPs:PVB (1:100, 3:100, and 5:100); (c) Typical images of PVB film and PVB/UCNPs hybrid film under the irradiation of 980 nm NIR light (2 W/cm^2).

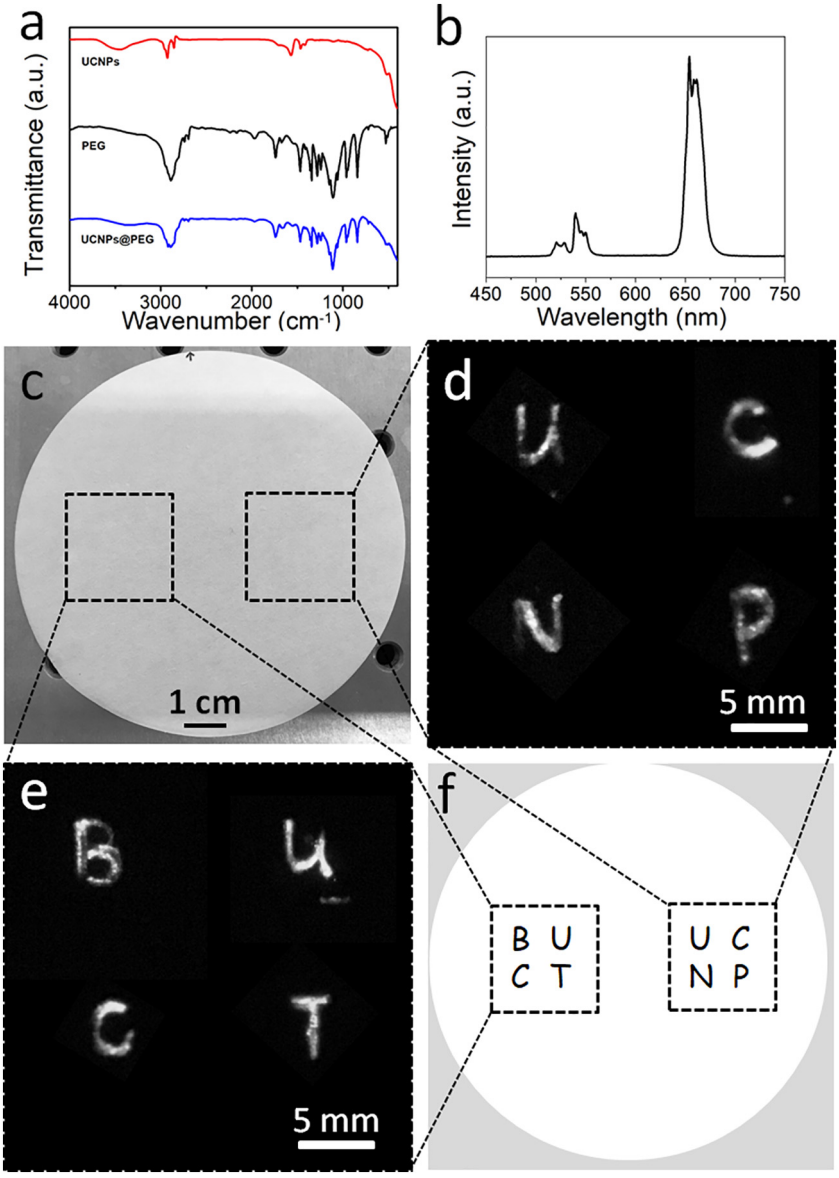

Fig. 7. (a) FTIR spectra of UCNPs, PEG and UCNPs@PEG. (b) Luminescence spectra of the aqueous nanodispersions of UCNPs@PEG under the 980 nm laser excitation. (c) Digital photos of a piece of paper with watermarks drawn with aqueous nanodispersions of $NaYF_4:Yb^{3+}/Er^{3+}$ under day light. (b–c) The upconversion luminescence imaging of the paper under irradiation of 980 nm NIR light (3.5 W/cm^2). (d) Schematic diagram of the watermarks.

All the films exhibited similar transmittance behavior in the range of 200–800 nm, indicating that $NaYF_4$:Yb^{3+}/Er^{3+} nanoparticles dispersed well in the PVB matrix with no significant aggregates. Although the two films are indistinguishable from each other in daylight, under the irradiation of 980 nm NIR light, the PVB/UCNPs hybrid film exhibited bright visible emission while no emission was observed from the pure PVB film (Fig. 6c). These results suggest the promising application of the PVB/UCNPs nanocomposites for anti-counterfeiting applications.

3.6. $NaYF_4$: Yb^{3+}/Er^{3+} nanodispersion for anti-counterfeiting

After phase-transfer treatment of the $NaYF_4$:Yb^{3+}/Er^{3+} nanoparticles by PEG coating, aqueous nanodispersions of UCNPs@PEG were prepared as anti-counterfeiting printing ink. Fig. 7a presents the FTIR spectra of UCNPs, PEG and UCNPs@PEG, demonstrating the successful coating of PEG on the surface of UCNPs. Fig. 7b showed the upvconversion luminescence spectra of UCNPs@PEG in water, which was similar as the luminescence spectra of UCNPs powders and dispersions in organic solvents (Figs. 4a and 5c), demonstrating that the phase-transfer treatment of the $NaYF_4$:Yb^{3+}/Er^{3+} caused no significant changes to the luminescence properties. Furthermore, we demonstrated the use of $NaYF_4$:Yb^{3+}/Er^{3+} nanodispersions to draw watermark by a pen on the commercially available paper. Fig. 7c shows a typical picture of the paper with "invisible" characters drawn by $NaYF_4$:Yb^{3+}/Er^{3+} nanodispersions under daylight. However, under the irradiation of 980 nm NIR light, the forgery-proof watermark images can be identified clearly, showing the characters of UCNP and BUCT (Fig. 7d–f). According to the long-term observation for two weeks, the watermarks adhered well to the paper and exhibited significant upconversion luminescence signals with no changes. These primary results demonstrated the potential of $NaYF_4$:Yb^{3+}/Er^{3+} nanodispersions for anti-counterfeiting in various substrates.

4. Conclusions

We demonstrate that the intensified mixing of the precursor by a high-gravity rotating packed bed reactor before the hydrothermal synthesis process enabled the preparation of ultrasmall $NaYF_4$:Yb^{3+}/Er^{3+} nanoparticles, without the need for stringent control over several experimental variables and additional of extra reactants. According to the morphology studies, the as-prepared $NaYF_4$: Yb^{3+}/Er^{3+} nanoparticles in RPB route exhibited much more uniform distribution and smaller size, than those obtained in the common STR route, due to the intensified mixing by the high-gravity RPB reactors. The upconversion luminescence spectra measurements indicated that Er^{3+}-doping levels were enhanced with the increased high-gravity levels. Various kinds of transparent $NaYF_4$:Yb^{3+}/Er^{3+} nanodispersions in organic solvents such as ethanol, acetone, tetrahydrofuran, ethyl acetate, chloroform, toluene and cyclohexane, as well as those in aqueous solution after phase-transfer treatment, were prepared, which exhibited bright upconversion luminescence under the 980 nm NIR light. Hybrid films of PVB/UCNPs were fabricated by a simple solution blending method using organic $NaYF_4$:Yb^{3+}/Er^{3+} nanodispersions. Anti-counterfeiting watermarks were drawn in paper using aqueous $NaYF_4$:Yb^{3+}/Er^{3+} nanodispersions. Under the 980 nm NIR light irradiation, upconversion luminescence signals in both materials could be identified clearly, demonstrating the potential of the RPB- derived highly dispersed $NaYF_4$:Yb^{3+}/Er^{3+} nanodispersions for anti-counterfeiting of various substrates. These preliminary findings should have important implications for the development of scalable synthesis methods for ultrasmall UCNPs and in moving toward robust UCNPs for commercialization. The "chemical engineering part" of nanoparticles story has only just begun [34]. Process intensification based on high gravity RPB reactors is promising for continuous and reproducible production of ultrasmall UCNPs. More related works, including the optimization of the experimental for high quality UCNPs, mechanistic aspects of shape control using different reactor types (such as spray-drying and microchannels devices), built-in analytical and feedback mechanisms for real-time tuning and optimization of products [35], are helpful to achieve high-quality UCNPs at scale, which should be good topics for future studies.

Acknowledgments

We are grateful for financial support from the National Key R & D Program of China (2017YFB0404302/2017YFB0404300), the National Natural Science Foundation of China (21808009), the Beijing Natural Science Foundation (2182051) and "111" project of China (B14004).

References

[1] G. Chen, H. Qiu, P.N. Prasad, X. Chen, Upconversion nanoparticles: design, nanochemistry, and applications in theranostics, Chem. Rev. 114 (2014) 5161–5214.
[2] X. Wang, R.R. Valiev, T.Y. Ohulchanskyy, H. Ågren, C. Yang, G. Chen, Dye-sensitized lanthanide-doped upconversion nanoparticles, Chem. Soc. Rev. 46 (2017) 4150–4167.
[3] D. Wang, L. Zhu, J. Chen, L. Dai, Liquid marbles based on magnetic upconversion nanoparticles as magnetically and optically responsive miniature reactors for photocatalysis and photodynamic therapy, Angew. Chem. Int. Ed. 55 (2016) 10795–10799.
[4] B. Zhou, B. Shi, D. Jin, X. Liu, Controlling upconversion nanocrystals for emerging applications, Nat. Nanotech. 10 (2015) 924–936.
[5] N.M. Sangeetha, P. Moutet, D. Lagarde, G. Sallen, B. Urbaszek, X. Marie, G. Viau, L. Ressier, 3D assembly of upconverting $NaYF_4$ nanocrystals by AFM nanoxerography: creation of anti-counterfeiting microtags, Nanoscale 5 (2013) 9587–9592.
[6] M. You, J. Zhong, Y. Hong, Z. Duan, M. Lin, F. Xu, Inkjet printing of upconversion nanoparticles for anti-counterfeit applications, Nanoscale 7 (2016) 4423–4431.
[7] M. You, M. Lin, S. Wang, X. Wang, G. Zhang, Y. Hong, Y. Dong, G. Jin, F. Xu, Three-dimensional quick response code based on inkjet printing of upconversion fluorescent nanoparticles for drug anti-counterfeiting, Nanoscale 8 (2016) 10096–10104.
[8] W. Zou, C. Visser, J.A. Maduro, M.S. Pshenichnikov, J.C. Hummelen, Broadband dye-sensitized upconversion of near-infrared light, Nat. Photon. 6 (2012) 560–564.
[9] Q. Zhan, H. Liu, B. Wang, Q. Wu, R. Pu, C. Zhou, B. Huang, X. Peng, H. Ågren, S. He, Achieving high-efficiency emission depletion nanoscopy by employing cross relaxation in upconversion nanoparticles, Nat. Commun. 8 (2017) 1058.
[10] Y. Liu, Y. Lu, X. Yang, X. Zheng, S. Wen, F. Wang, X. Vidal, J. Zhao, D. Liu, Z. Zhou, C. Ma, J. Zhou, J.A. Piper, P. Xi, D. Jin, Amplified stimulated emission in upconversion nanoparticles for super-resolution nanoscopy, Nature 543 (2017) 229–233.
[11] D. Wang, L. Zhu, Y. Pu, J.-X. Wang, J.-F. Chen, L. Dai, Transferrin-coated magnetic upconversion nanoparticles for efficient photodynamic therapy with near-infrared irradiation and luminescence bioimaging, Nanoscale 9 (2017) 11214–11221.
[12] N.M. Idris, M.K. Gnanasammandhan, J. Zhang, P.C. Ho, R. Mahendran, Y. Zhang, *In vivo* photodynamic therapy using upconversion nanoparticles as remote-controlled nanotransducers, Nat. Med. 178 (2012) 1580–1585.
[13] X. Huang, S. Han, W. Huang, X. Liu, Enhancing solar cell efficiency: the search for luminescent materials as spectral converters, Chem. Soc. Rev. 42 (2013) 173–201.
[14] S.K. MacDougall, A. Ivaturi, J. Marques-Hueso, K.W. Krämer, B.S. Richards, Ultra-high photoluminescent quantum yield of β-$NaYF_4$:10% Er^{3+} *via* broadband excitation of upconversion for photovoltaic devices, Opt. Express 20 (2012) A879–A887.
[15] M. He, X. Pang, X. Liu, B. Jiang, Y. He, H. Snaith, Z. Lin, Monodisperse dual-functional upconversion nanoparticles enabled near-infrared organolead halide perovskite solar cells, Angew. Chem. Int. Ed. 55 (2016) 4280–4284.
[16] M.K. Tsang, G. Bai, J. Hao, Stimuli responsive upconversion luminescence nanomaterials and films for various applications, Chem. Soc. Rev. 44 (2015) 1585–1607.
[17] D. Wang, Z. Wang, Q. Zhan, Y. Pu, J.-X. Wang, N.R. Foster, L. Dai, Facile and scalable preparation of fluorescent carbon dots for multifunctional applications, Engineering 3 (2017) 402–408.
[18] Y. Liu, K. Ai, L. Lu, Designing lanthanide-doped nanocrystals with both up-and down-conversion luminescence for anti-counterfeiting, Nanoscale 3 (2011) 4804–4810.
[19] J.-F. Chen, Green Chemical Engineering, 3, 2017 283–284.
[20] J.C. Boyer, F. Vetrone, L.A. Cuccia, J.A. Capobianco, Synthesis of colloidal upconverting $NaYF_4$ nanocrystals doped with Er^{3+}, Yb^{3+} and Tm^{3+}, Yb^{3+} *via* thermal decomposition of lanthanide trifluoroacetate precursors, J. Am. Chem. Soc. 128 (2006) 7444–7445.
[21] X. Ye, J.E. Collins, Y. Kang, J. Chen, D.T.N. Chen, A.G. Yodh, C.B. Murray, Morphologically controlled synthesis of colloidal upconversion nanophosphors and their shape-directed self-assembly, Proc. Natl. Acad. Sci. U. S. A. 107 (2010) 22430–22435.
[22] J.H. Zeng, J. Su, Z.H. Li, R.X. Yan, Y.D. Li, Synthesis and upconversion luminescence of hexagonal-phase $NaYF_4$: Yb, Er^{3+} phosphors of controlled size and morphology, Adv. Mater. 17 (2005) 2119–2123.
[23] Y. Pu, J. Leng, D. Wang, J.-X. Wang, N.R. Foster, J.-F. Chen, Recent progress in the green synthesis of rare-earth doped upconversion nanophosphors for optical bioimaging from cells to animals, Chin. J. Chem. Eng. (2018)https://doi.org/10.1016/j.cjche.2018.03.005.
[24] Z. Mao, C. Yang, Micro-mixing in chemical reactors: a perspective, Chin. J. Chem. Eng. 25 (2017) 381–390.

[25] H. Zhao, L. Shao, J. Chen, High-gravity process intensification technology and application, Chem. Eng. J. 156 (2010) 588–593.
[26] F. Wang, Y. Han, C.S. Lim, Y. Lu, J. Wang, J. Xu, H. Chen, C. Zhang, M. Hong, X. Liu, Simultaneous phase and size control of upconversion nanocrystals through lanthanide doping, Nature 463 (2010) 1061–1065.
[27] B. Lv, L. Zhao, Y. Pu, Y. Le, X. Zeng, J. Chen, N. Wen, J.-X. Wang, Facile preparation of controllable-aspect-ratio hydroxyapatite nanorods with high-gravity technology for bone tissue engineering, Ind. Eng. Chem. Res. 56 (2017) 2976–2983.
[28] X. Yang, J. Leng, D. Wang, Z. Wang, J.-X. Wang, Y. Pu, J. Shui, J.-F. Chen, Synthesis of flower-shaped V_2O_5: Fe^{3+} microarchitectures in a high-gravity rotating packed bed with enhanced electrochemical performance for lithium ion batteries, Chem. Eng. Process. 120 (2017) 201–206.
[29] J. Chen, Y. Wang, F. Guo, X. Wang, C. Zheng, Synthesis of nanoparticles with novel technology: high-gravity reactive precipitation, Ind. Eng. Chem. Res. 39 (2010) 948–954.
[30] Y. Pu, L. Lin, D. Wang, J.-X. Wang, J. Qian, J.-X. Chen, Green synthesis of highly dispersed ytterbium and thulium co-doped sodium yttrium fluoride microphosphors for *in situ* light upconversion from near-infrared to blue in animals, J. Colloid Interface Sci. 511 (2018) 243–250.
[31] J. Leng, J. Chen, D. Wang, J.-X. Wang, Y. Pu, J.-F. Chen, Scalable preparation of Gd_2O_3: Yb^{3+}/Er^{3+} upconversion nanophosphors in a high-gravity rotating packed bed reactor for transparent upconversion luminescent films, Ind. Eng. Chem. Res. 56 (2017) 7977–7983.
[32] S. Xu, Z. Yang, G. Wang, S. Dai, J. Zhang, L. Hu, Z. Jiang, Optical transitions and upconversion mechanisms in Er 3± doped heavy metal oxyfluoride germanate glass, J. Alloys Compd. 377 (2004) 253–258.
[33] D. Marani, C. Gadea, J. Hjelm, P. Hjalmarsson, M. Wandel, R. Kiebach, Influence of hydroxyl content of binders on rheological properties of cerium-gadolinium oxide (CGO) screen printing inks, J. Eur. Ceram. Soc. 35 (2015) 1495–1504.
[34] Y. Pu, F. Cai, D. Wang, J.-X. Wang, J.-F. Chen, Colloidal synthesis of semiconductor quantum dots toward large-scale production: a review, Ind. Eng. Chem. Res. 57 (2018) 1790–1802.
[35] F. Cai, D. Wang, M. Zhu, S. He, Pencil-like imaging spectrometer for bio-samples sensing, Biomed. Opt. Express 8 (2017) 5427–5436.